

FoSp: Focus and Separation Network for Early Smoke Segmentation

Lujian Yao, Haitao Zhao, Jingchao Peng, Zhongze Wang, Kaijie Zhao
Automation Department, School of Information Science and Engineering,
East China University of Science and Technology

Abstract

Early smoke segmentation (ESS) enables the accurate identification of smoke sources, facilitating the prompt extinguishing of fires and preventing large-scale gas leaks. But ESS poses greater challenges than conventional object and regular smoke segmentation due to its small scale and transparent appearance, which can result in high miss detection rate and low precision. To address these issues, a Focus and Separation Network (FoSp) is proposed. We first introduce a Focus module employing bidirectional cascade which guides low-resolution and high-resolution features towards mid-resolution to locate and determine the scope of smoke, reducing the miss detection rate. Next, we propose a Separation module that separates smoke images into a pure smoke foreground and a smoke-free background, enhancing the contrast between smoke and background fundamentally, improving segmentation precision. Finally, a Domain Fusion module is developed to integrate the distinctive features of the two modules which can balance recall and precision to achieve high F_β . Furthermore, to promote the development of ESS, we introduce a high-quality real-world dataset called SmokeSeg, which contains more small and transparent smoke images than the existing datasets. Experimental results show that our model achieves the best performance on three available datasets: SYN70K ($mIoU$: 83.00%), SMOKE5K (F_β : 81.6%) and SmokeSeg (F_β : 72.05%). Especially, our FoSp outperforms SegFormer by 7.71% (F_β) for early smoke segmentation on SmokeSeg.

1. Introduction

In wildlife, smoke is an important indicator of fire. Early smoke segmentation (ESS) enables rapid identification of the location of the fire [13, 18], facilitating the timely extinguishing of the flames by rescue personnel and preventing the occurrence of large fires. In industrial production, ESS can also aid in promptly detecting the location of gas leaks and prevent the spread of toxic and harmful gases [4].

Smoke segmentation presents a more challenging task than ordinary object segmentation. Unlike conventional

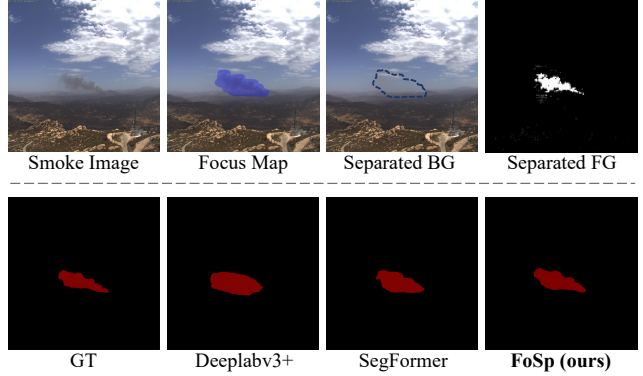


Figure 1. **Process and Comparison.** A Focus Map is generated by the proposed *Focus* module to determine the smoke scope. Then, we introduce a *Separation* module to extract the *smoke foreground* (Separated FG) from the *smoke-free background* (Separated BG), thus enhancing the contrast between the foreground and the background. This method leads to obtaining a more *refined* smoke map than strong baselines like DeepLabV3+[1] and SegFormer[26].

objects, which are typically rigid and have clear edges, smoke is a non-rigid substance with ever-changing form and blurred edges. Furthermore, early smoke segmentation is much more challenging than regular smoke segmentation, as early smoke is small and transparent, resulting in *high miss detection rate* (incomplete segmentation) and *low precision* (rough-edge segmentation). Previous regular smoke segmentation methods [33, 34, 35] primarily emphasize larger receptive fields to cope with the variability and blurred edges of smoke. However, these methods do not work well for identifying early smoke with small scale and transparent appearance.

To address the issue of early smoke, we propose a *Focus and Separation Network* (FoSp) which concentrates on the formulation of smoke images. Firstly, we design a *Focus* module utilizing bidirectional cascade which directs low-resolution and high-resolution features towards mid-resolution to locate and confirm the scope of smoke, effectively reducing the *miss detection rate*. Subsequently, we propose a *Separation* module that separates smoke images into a pure smoke foreground and a smoke-free background, increasing the contrast between smoke and back-

ground to improve the *precision* of segmentation. Finally, we integrate the distinctive features of the two modules and develop a *Domain Fusion* module that balances *recall* and *precision* to obtain the general F_β .

Specifically, 1) *Focus module*: We propose a Bidirectional Cascade Generator (BCG) for focus module. BCG employs bidirectional guidance of low-resolution and high-resolution features, targeting respectively the smoke body and the smoke edge, towards mid-resolution features to generate a Focus Map (FM) that can fully encompass the smoke region. 2) *Separation module*: In order to retain information and maintain consistency with high-level segmentation tasks, we adopt a feature-level approach to separate the foreground and background of smoke images. By utilizing FM, we acquire the smoke region and adopt the inpainting technique to complete the smoke area with regular smoke-free background, using the adjacent environment (especially the area surrounding the smoke) as a reference. We subsequently deduct the smoke-free background from the initial smoke region to obtain the separated smoke foreground. 3) *Domain Fusion*: Since the foreground features are generated by the inpainter (inpainting model), the origin features and foreground features actually belong to distinct feature domains. An MLP at each stage is designed to hierarchically merge the features from two domains.

Furthermore, we provide a large and real-world dataset called SmokeSeg, which includes 6,144 real images of smoke, with a considerable number of them featuring small and transparent smoke. SmokeSeg currently boasts the largest number of real images among publicly available smoke segmentation datasets. Notably, the SmokeSeg contains 4.5 times more real images than SMOKE5K [29], which only comprises 1,360 real images.

Our main contributions can be summarized as follows:

- We propose a Focus and Separation Network (FoSp), where the Focus module and Separation module are introduced to reduce the miss detection rate and improve precision of early smoke segmentation, respectively.
- We have created a large-scale dataset named *SmokeSeg* for early smoke segmentation, which includes 6144 real images with pixel-wise annotations.
- Our FoSp achieve the best performance on three datasets: SYN70K ($mIoU$: 83.00%), SMOKE5K (F_β : 81.6%) and SmokeSeg (F_β : 72.05%). Particularly, FoSp surpasses SegFormer by 7.71% (F_β) for early smoke segmentation on SmokeSeg.

2. Related Work

In this section, we begin by reviewing smoke segmentation methods that are based on both traditional and deep learning approaches. Subsequently, we provide a brief

overview of prior attention and conclude by summarizing current status of smoke segmentation datasets.

Early Smoke Segmentation: Although current semantic segmentation methods [1, 19, 26] are effective at segmenting regular objects (i.e., those with clear outlines and roughly the same shape), these generic algorithms are not suitable for early smoke segmentation due to its varying transparency and small scale. Traditional smoke segmentation methods have mainly focused on extracting high-quality color and texture features [11, 28, 32], and deep-learning-based methods [33, 34, 35] mainly focus on extracting features with larger receptive fields to handle the variability and blurred edges of smoke. However, these methods suffer from high miss detection rate and low precision in segmenting small and transparent early smoke. And many of them [34, 35] have only been quantitatively evaluated on synthetic datasets. Despite some methods [7, 21] claiming to address early smoke, they still rely on images of regular smoke. Therefore, the existing smoke segmentation methods are not capable of effectively addressing the issue of early smoke.

Prior Attention: Prior attention is a mechanism that adds a branch to the network before the backbone [20, 23, 27] or before the final predictions [14, 30], making the network focus on a specific area of the image in early to obtain finer predictions. However, current methods are mostly used for object detection and are designed to improve *precision*. How to obtain a prior attention for segmentation with high *recall* is still to be resolved.

Smoke Segmentation Datasets: Currently, there are two main smoke segmentation datasets: SYN70K [35] and SMOKE5K [29]. SYN70K is a synthetic dataset comprising 70k images, while SMOKE5K contains 1k real images and 4k synthetic images, with the latter being selected from SYN70K. However, neither of these datasets is specifically designed for early smoke segmentation. The SYN70K comprises entirely of synthetic smoke, which is larger in scale and significantly different from real images. The SMOKE5K has only a small number of real smoke images and a low proportion of early small and transparent smoke. Therefore, there is currently no dataset particularly designed for early smoke segmentation.

3. Method

In this section, we first present a general introduction of our FoSp. Then we describe the three modules of FoSp: Focus module, Separation module and Domain Fusion module. Finally, we present the loss function used to train our model.

3.1. Introduction of Focus and Separation (FoSp)

Intuition. We assume that the smoke image $\mathbf{I} \in \mathbb{R}^{H \times W \times 3}$ is composed of a smoke-free background $\mathbf{B} \in \mathbb{R}^{H \times W \times 3}$

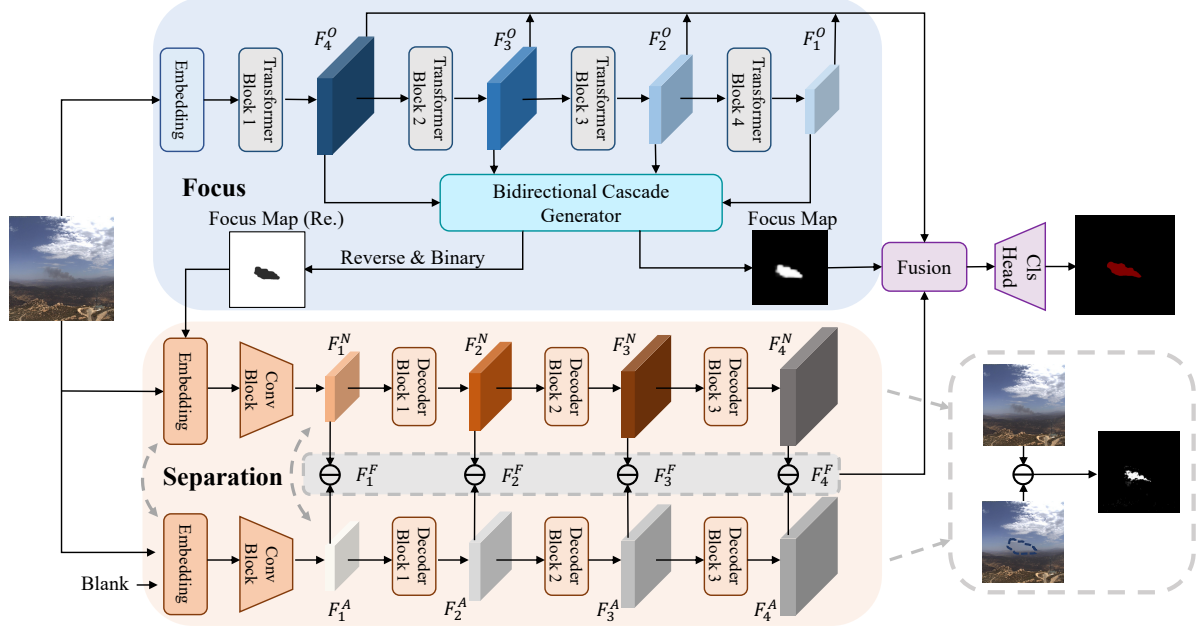


Figure 2. **The structure of our FoSp.** The Focus module extracts image features and generates a Focus Map using Bidirectional Cascade Generator (BCG). The Separation module consists of two inpainters: one to complete the smoke areas with smoke-free backgrounds using the original image and Focus Map, and the other using the original image and a blank image. The smoke foreground features are obtained by subtracting the two features, and then the origin features, Focus Map, and foreground features are fused in the Domain Fusion module to obtain the final prediction.

and a smoke foreground $\mathbf{S} \in \mathbb{R}^{H \times W \times 3}$:

$$\mathbf{I} = (1 - \alpha) \odot \mathbf{B} + \alpha \odot \mathbf{S}, \quad (1)$$

where \odot indicates the element-wise multiplication and the $\alpha \in \mathbb{R}^{H \times W \times 3}$ is used to control the density of the smoke foreground in RGB channels. Supposing we can obtain a smoke-free background image \mathbf{B} , we are capable of enhancing the smoke foreground \mathbf{S} fundamentally by controlling the value of α to obtain a precise segmentation map. Following such intuition, we propose a *Focus and Separation Network* (FoSp).

Overview. As shown in Fig. 2, we first propose a Focus module to locate and confirm the scope of smoke. This enables the network to pay closer attention to the smoke and reduce the miss detection rate. Next, a Separation module is introduced to split the smoke image into pure smoke foreground and smoke-free background, which fundamentally enhances the contrast between the foreground and background, thereby improving precision. Finally, a Domain Fusion module is developed to narrow the domain gap between the features generated by the first two modules, ultimately achieving a balance between recall and precision.

3.2. Focus Module

Intuition. Most segmentation methods use pyramid-based *unidirectional* feature integration to obtain a more refined prediction. However, our Focus module is designed to

achieve a more complete smoke area. To achieve this, we introduce a novel *bidirectional* feature cascade approach. We consider the smoke as two parts: the low-opacity smoke body and the high-opacity smoke edge. As shown in Fig. 3, low-resolution features can provide an approximate outline of smoke body. However, the effectiveness of capturing transparent regions of smoke is compromised. Conversely, high-resolution features offer a more precise attention and can identify transparent parts of smoke edge, but cannot fully capture the entire smoke. Therefore, we propose a bidirectional fusion of features which can integrate features from both low and high resolution, resulting in a complete scope of the smoke.

Overview. In the focus module, a Bidirectional Cascade Generator (BCG) is proposed to integrate the original multi-scale image features for locating and confirming the range of smoke, which we refer to as the Focus Map (FM). As show in Fig. 3, BCG bidirectionally guides low-resolution features and high-resolution features towards mid-resolution to obtain a complete scope of smoke.

Detail. As shown in Fig 2, in the feature extraction section, MiT-B3 [26] is adopted as our backbone, which is a transformer-based backbone with large receptive field that can handle the variability of smoke. Specifically, we pre-process the image using an embedding layer and extract features at four different scales using four Transformer blocks. These scales range from small to large and are respectively $\mathbf{F}_i \in \mathbb{R}^{\frac{H}{2^{i-1}} \times \frac{W}{2^{i-1}} \times C_i}$ ($i = 1, 2, 3, 4$). The BCG is illus-

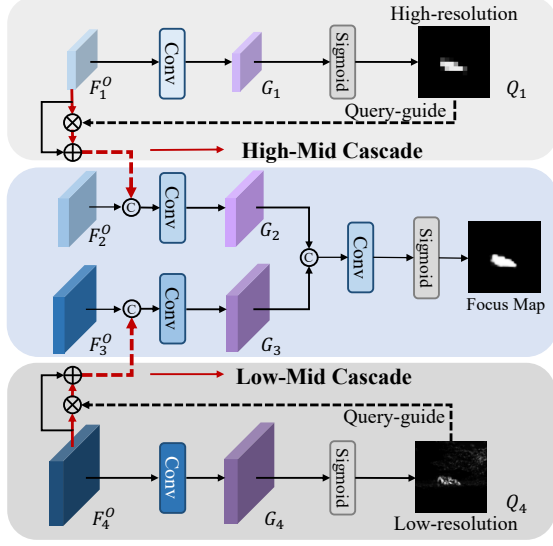


Figure 3. **The structure of Bidirectional Cascade Generator.** It guides low-resolution features and high-resolution features towards mid-resolution to obtain a more complete scope of smoke.

trated in Fig. 3, which consists of two parts: Low-Mid Cascade (LMC) and High-Mid Cascade (HMC). The two modules are similar, so we will use the LMC module as an example to explain. In LMC, The lowest-resolution feature $F_1 \in \mathbb{R}^{\frac{H}{32} \times \frac{W}{32} \times 1}$ is fed into a layer of Conv to obtain the logits $G_1 \in \mathbb{R}^{\frac{H}{32} \times \frac{W}{32} \times 1}$ and then applied the Sigmoid function to obtain the prediction $Q_1 \in \mathbb{R}^{\frac{H}{32} \times \frac{W}{32} \times 1}$ of the F_1 . A query-guide approach is adopted to enhance the feature maps by taking the dot product of Q_1 and F_1 , and adding the result to the F_1 . The cascade process of obtaining the final output logits $G_2 \in \mathbb{R}^{\frac{H}{16} \times \frac{W}{16} \times 1}$ of LMC can be represented using the following equation:

$$G_2 = \text{Conv}(\text{Cat}(U(Q_1 * F_1 + F_1), F_2), \theta_2), \quad (2)$$

where the θ_2 is the learnable parameters of the Conv. The HMC follows the same procedure to obtain the final logits $G_3 \in \mathbb{R}^{\frac{H}{8} \times \frac{W}{8} \times 1}$. At last, the two intermediate resolution logits G_2 (LMC) and G_3 (HMC) are fused to obtain the final Focus Map ($FM \in \mathbb{R}^{\frac{H}{16} \times \frac{W}{16} \times 1}$).

$$FM = \text{Sigmoid}(\text{Conv}(\text{Cat}(G_2, G_3), \theta_m)), \quad (3)$$

where the θ_m is the learnable parameters of the Conv.

3.3. Separation Module

Intuition. The region of FM shares similarities with the adjacent pixels, while the region of smoke can be perceived as an external element that is not compatible with the background. We leverage the contextual features surrounding FM to complement the features within the FM area, thereby aligning them with the neighboring features (i.e., smoke-free background). Consequently, by subtracting the original image, the foreground smoke can be extracted.

Overview. In Separation module, we utilize the FM to obtain the smoke region and apply the inpainting technique (a.k.a Image completion) to fill the smoke area with smoke-free background using the surrounding scene (particularly the area around the smoke) as a reference. We then subtract the smoke-free background from the original smoke region to derive the pure smoke foreground. Furthermore, to preserve information and maintain consistency with high-level segmentation tasks, we separate the foreground and background at the *feature level*.

Detail. As shown in Fig. 2, In order to separate the foreground and background of smoke images at the feature level, the entire Separation module is composed of two weight-shared inpainters.

1) In the top branch, the original image I and Focus Map FM are first input into the embedding layer $EB(\cdot)$ for feature integration and then encoded into a latent feature $F_1^N \in \mathbb{R}^{\frac{H}{32} \times \frac{W}{32} \times C_1}$ through the Conv block.

$$F_1^N = \text{Conv}(EB(I, FM), \theta_I), \quad (4)$$

where θ_I represents the pre-trained Conv parameters of the inpainting network.

2) Different from the top branch, in the bottom branch, the input is the original image I and a Blank image, without any mask.

$$F_1^A = \text{Conv}(EB(I, \text{Blank}), \theta_I), \quad (5)$$

where $F_1^A \in \mathbb{R}^{\frac{H}{32} \times \frac{W}{32} \times C_1}$.

3) Then the latent features of the two branches are sent to three decoder blocks and three different scale inpainting-network-domain feature maps are obtained.

$$F_i^{A/N} = \text{Dec}_{i-1}(F_{i-1}^{A/N}), i = 2, 3, 4, \quad (6)$$

where $F_i^{A/N} \in \mathbb{R}^{\frac{H}{2^{6-i}} \times \frac{W}{2^{6-i}} \times C_i}$.

4) Finally, we calculate the L^1 -norm of the four scale feature maps in both the top branch and the bottom branch to get the foreground features F_i^F , forming a feature list and feeding it into the Domain Fusion module.

$$F_i^F = \beta * \|F_i^N - F_i^A\|_1, i = 1, 2, 3, 4 \quad (7)$$

where β is the gain factor and we set $\beta = 10$.

3.4. Domain Fusion

Intuition. Due to the foreground features generated by the inpainters, the origin features and foreground features actually belong to different feature domains. Simply adding features does not effectively merge the high-quality features of both, and this operation may even damage the original feature domain due to different information represented by different channels. Therefore, we design Domain Fusion module to achieve the fusion of both domain features.

Detail. As shown in Fig. 4, the Domain Fusion module is divided into three domains: origin domain, foreground domain, and fusion domain. The origin domain is composed

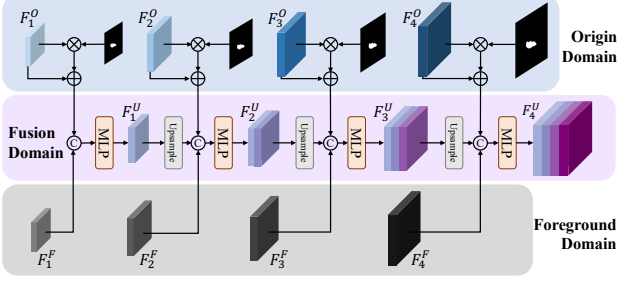


Figure 4. **The structure of our Domain Fusion Module.** At each stage, the features of the two domains and the feature of previous fusion stage are combined through concatenation and then integrated using an MLP, resulting in a hierarchical merging of the features from both domains.

of features at different scales generated by the Focus module, and we utilize the Focus Map to enhance the features of the smoke region. The foreground domain is composed of four distinct scale foreground features generated by the Separation module. In each stage, the features of the two domains and the feature of *previous fusion stage* are concatenated and then fused with an MLP. The features of the two domains are hierarchically merged in this way.

3.5. Loss Function

The loss function consists of two parts: base loss and *Focus* loss. In conjunction with our proposed Focus module, we introduce a *Focus* loss, which provides supervisory information to the prediction logits $\mathbf{G}_i (i = 1, 2, 3, 4)$ of multiple resolution feature maps.

$$\mathcal{L}_{focus} = \lambda_f \mathcal{L}_{BCE}(\mathbf{FM}, \mathcal{Y}) + \sum_{i=1}^4 \lambda_i (\mathcal{L}_{BCE}(\mathbf{G}_i, \mathcal{Y})), \quad (8)$$

where \mathcal{L}_{BCE} is the binary cross-entropy, \mathcal{Y} is the ground truth, λ_f and λ_i are the weighting factors and we set $\lambda_f = \lambda_i = 0.1$.

For the basic segmentation loss, we use the standard binary cross-entropy. And the final objective function is the sum of the two loss:

$$\mathcal{L} = \mathcal{L}_{focus} + \lambda_b \mathcal{L}_{BCE}(\mathbf{P}, \mathcal{Y}), \quad (9)$$

where \mathbf{P} is the final prediction of model, λ_b is the weighting factor and we set $\lambda_b = 0.5$.

4. Experiments

In this section, we first introduce our SmokeSeg dataset and training settings. Then, we compare our method with others on three datasets. Next, the ablation experiments are performed on FoSp. Finally, we further investigate some specific modules in more detail.

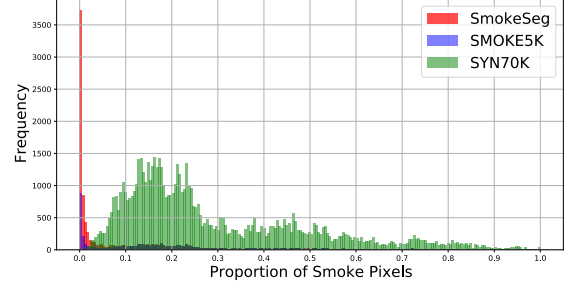


Figure 5. **Distribution map of smoke pixel ratio in an image of three datasets.** The distribution of our SmokeSeg is significantly skewed to the left. This indicates that SmokeSeg contains a much higher proportion of small smoke images than other two datasets.

4.1. SmokeSeg Dataset

There are two main smoke segmentation datasets available: SYN70K [35] and SMOKE5K [29]. SYN70K comprises 70k synthetic images, while SMOKE5K is a dataset containing 1,360 real images and 4k synthetic images, with the latter being selected from SYN70K. However, neither of these datasets is tailored specifically for *early smoke segmentation*. SYN70K is a synthetic dataset with lots of images of smoke, but the smokes in it are large and prominent, which are quite different from real smoke. SMOKE5K has a limited number of real smoke images, and a low proportion of these are early smoke images, making it difficult to conduct experiments specifically targeted early smoke segmentation.

To address these issues and further promote the development of early smoke segmentation, we contribute *SmokeSeg* dataset. SmokeSeg consists of 6,144 real images (the raw smoke images are sourced from FigLib [2].), which has the largest number of real images with pixel-wise annotations in any publicly available smoke segmentation dataset. The number of real images in SmokeSeg is 4.5 times larger than that of SMOKE5K, which only comprises 1,360 real images. The majority of these images in SmokeSeg are early smoke, characterized by small scale and transparent appearance. Fig. 5 shows the distribution of smoke pixel ratios in three datasets, with smaller ratios indicating smaller smoke. It can be seen that the SYN70K dataset hardly contains small smoke images, while SMOKE5K only has a little fraction of them. In contrast, the majority of our SmokeSeg dataset is composed of small smoke images.

4.2. Implementation Details

Datasets. We conduct experiments on three large smoke datasets: SYN70K [35], SMOKE5K [29] and our SmokeSeg. To make a fair comparison, we train our models on SYN70K and SMOKE5K and test them on their respective test sets. And then we provide a new benchmark on our SmokeSeg dataset.

Evaluation Metrics. Following previous smoke segmentation literature [29, 35], we evaluate our model utilizing the mMse (\mathcal{M}) and $mIoU$ metric on SYN70K and adopt mMse (\mathcal{M}) and F-measure (F_β) on SMOKE5K. For our *SmokeSeg*, we employ the *three metrics* mentioned above (F_β , $mIoU$, \mathcal{M}) to comprehensively evaluate the performance of the model.

Training Details. Each image is resize to 512×512 . Random crop and random flip are adopted during the training. We use the AdamW [10] optimizer and set the learning rate to $6e-5$ with 0.01 weight decay. We train 40k iterations on SMOKE5K and *SmokeSeg*, and 80k iterations on SYN70K, with all batch size set to 6. The code can be found in the supplementary materials.

4.3. Comparison with State-of-the-Art Methods

SYN70K [35]. We evaluate our model on their three synthetic test sets (DS01, DS02, and DS03). As shown in Table 1, our model outperforms previous state-of-the-art method Trans-BVM [29] on all three test sets, with significant improvement (The $\mathcal{M} \downarrow$ have decreased by 2.81% on DS02 test set.).

	DS01		DS02		DS03	
Method	$\mathcal{M} \downarrow$	$mIoU \uparrow$	$\mathcal{M} \downarrow$	$mIoU \uparrow$	$\mathcal{M} \downarrow$	$mIoU \uparrow$
SMD [22]	0.3209	62.88	0.3379	61.50	0.3255	62.09
TBFCN [39]	0.3021	66.67	0.3196	65.85	0.3070	66.20
LRN [6]	0.3069	66.43	0.3078	67.71	0.3041	67.46
HG-Net2 [15]	0.3186	64.27	0.3380	63.06	0.3273	64.18
HG-Net8 [15]	0.3187	62.10	0.3301	61.89	0.3215	62.45
ESPNet [12]	-	61.85	-	61.90	-	62.77
LKM [16]	0.2658	75.82	0.2799	74.93	0.2748	75.39
RefineNet [8]	0.2486	77.16	0.2590	76.75	0.2515	77.52
PSPNet [40]	0.2366	78.71	0.2480	78.01	0.2430	78.39
CCL [3]	0.2349	78.87	0.2498	77.95	0.2429	78.55
DFN [31]	0.2269	80.87	0.2411	79.90	0.2332	80.60
DSS [35]	0.2745	71.04	0.2894	70.01	0.2861	69.81
W-Net [34]	0.2688	73.06	0.2548	73.97	0.2596	73.36
CCENet [33]	-	74.67	-	75.24	-	76.01
Trans-BVM [29]	0.1210	-	0.1362	-	0.1291	-
FoSp (ours)	0.1026	83.00	0.1081	81.81	0.1048	82.80

Table 1. Performance on three test sets of SYN70K

SMOKE5K [29]. We evaluate our model on their test set of 400 real smoke images. As demonstrated in Table 2, our approach surpasses previous state-of-the-art Trans-BVM [29] and achieves 2.5% improvement on F_β .

SmokeSeg. As there is no complete open source smoke segmentation training code available, we have chosen several strong baselines that perform well in semantic segmentation for comparison. In order to better explore the recognition abilities of various methods for smoke of different scales, especially for early smoke, we divide the test set into three parts based on the proportion of smoke pixels in an image, namely small, medium, and large, and test them separately. We use the evaluation metric on "small" to mea-

Method	$F_\beta \uparrow$	$\mathcal{M} \downarrow$
F3Net [24]	67.0	0.004
BASNet [17]	73.3	0.005
SCRN [25]	76.9	0.003
ITSD [41]	77.4	0.003
UCNet [38]	78.7	0.003
Trans-BVM [29]	79.1	0.002
FoSp (ours)	81.6	0.002

Table 2. Performance on the test set of SMOKE5K.

sure the *early smoke segmentation capability* of our model.

$$\begin{cases} \text{Small : } \delta < 0.5\% \\ \text{Medium : } 0.5\% < \delta < 2.5\% \\ \text{Large : } \delta > 2.5\% \end{cases}, \quad (10)$$

where δ is the smoke pixel ratio in an image. In addition, to ensure the segmentation performance on large smoke, we also incorporated 4k synthetic smoke images into the training process.

As shown in Table 3, the comparison is divided into two parts, with the top part of the table showing the comparison of methods with lightweight backbones, and the bottom part showing the comparison of methods with medium-sized backbones. From the comparison of the lightweight methods, our FoSp using the least number of parameters surpasses other methods with higher parameter counts in the vast majority of cases. In the comparison of the medium-sized methods, our FoSp significantly outperforms all other methods, especially in the comparison of *small smoke*, where our method is 7.71% higher than the second-best SegFormer [26] on F_β , demonstrating that our method can better recognize early smoke.

4.4. Ablation Study

To further investigate the role of each module in our proposed FoSp, we conduct ablation experiments on the *SmokeSeg* dataset. As shown in Table 4, we utilize SegFormer [26] as the baseline for our study. In order to investigate the influence of individual modules on the miss detection rate and precision of early smoke detection, we augment the evaluation metrics by including recall (for miss detection rate) and precision. F_β is adopted as the comprehensive evaluation metric.

Effect of Focus Module. Methods (b) and (c) in Table 4 demonstrate the role of the Focus loss and Focus module. It can be observed that after incorporating the Focus loss and Focus module, a substantial enhancement on recall is observed, particularly in the segmentation of small smoke particles, where the recall increased by 7.70% compared to the baseline. As illustrated in Fig. 6, high-resolution features can capture fine details of the smoke edges, whereas low-resolution features can capture the overall characteristics of the smoke body. By establishing bidirectional cascade between these two types of features, a Focus map can

	Total			Small			Medium			Large			
Method	$F_\beta \uparrow$	$mIoU \uparrow$	$\mathcal{M} \downarrow$	$F_\beta \uparrow$	$mIoU \uparrow$	$\mathcal{M} \downarrow$	$F_\beta \uparrow$	$mIoU \uparrow$	$\mathcal{M} \downarrow$	$F_\beta \uparrow$	$mIoU \uparrow$	$\mathcal{M} \downarrow$	Params (M)
FCN-s [9]	54.12	42.06	0.0105	33.93	25.00	0.0017	64.08	50.65	0.0051	67.24	52.96	0.0271	9.71
DeepLabv3+-s [1]	59.56	46.71	0.0095	44.06	32.77	0.0014	68.35	54.76	0.0046	68.37	54.46	0.0246	15.23
PSPNet-s [40]	57.28	44.76	0.0096	40.86	30.70	0.0015	63.77	50.09	0.0051	69.72	55.68	0.0245	13.61
OCRNet-s [36]	62.64	50.11	0.0087	50.99	39.47	0.0013	71.47	55.09	0.0043	70.45	57.33	0.0225	12.07
SegFormer-s [26]	60.73	48.19	0.0097	48.21	35.18	0.0015	70.22	56.81	0.0042	67.52	54.18	0.0256	6.38
FoSp-s (ours)	64.26	51.44	0.0089	51.35	39.57	0.0012	72.47	58.95	0.0041	70.60	57.31	0.0234	5.79
FCN [9]	65.41	51.89	0.0089	55.30	41.58	0.0013	70.72	57.31	0.0043	71.64	58.22	0.0233	49.48
PSPNet [40]	65.80	52.42	0.0086	55.27	42.01	0.0012	71.44	58.13	0.0042	72.15	58.54	0.0224	48.96
EncNet [37]	66.54	53.15	0.0088	58.09	44.86	0.0012	71.16	57.74	0.0042	71.54	57.96	0.0232	35.87
DeepLabv3+ [1]	67.26	53.85	0.0084	57.00	43.70	0.0013	73.34	59.80	0.0039	72.79	59.39	0.0219	43.58
CCNet [5]	64.45	51.42	0.0090	52.94	40.59	0.0015	69.79	56.26	0.0046	72.31	59.01	0.0231	49.81
OCRNet [36]	65.13	52.66	0.0085	52.60	41.04	0.0012	72.24	59.34	0.0039	72.25	59.16	0.0224	70.37
SegFormer [26]	67.99	54.98	0.0088	58.32	45.72	0.0017	74.34	61.37	0.0038	72.50	58.95	0.0235	44.60
FoSp (ours)	72.05	59.03	0.0079	66.03	52.68	0.0010	75.90	62.99	0.0037	74.98	62.24	0.0208	47.52

Table 3. Performance on the test set of SmokeSeg.

	Module					Metrics		Metrics (small)			
Method	Baseline	\mathcal{L}_{focus}	Focus	Separation	Domain Fusion	Recall \uparrow	Precision \uparrow	$F_\beta \uparrow$	Recall \uparrow	Precision \uparrow	$F_\beta \uparrow$
(a)	✓					71.77	71.34	67.99	60.82	63.29	58.32
(b)	✓	✓				73.53	71.55	68.90	65.06	63.06	60.99
(c)	✓	✓	✓			75.60	71.50	70.00	68.52	62.86	62.23
(d)	✓	✓	✓	✓		73.82	75.50	71.50	66.24	71.16	65.77
(e)	✓	✓	✓	✓	✓	74.60	75.20	72.05	68.24	68.56	66.03

Table 4. Ablation study of our FoSp.

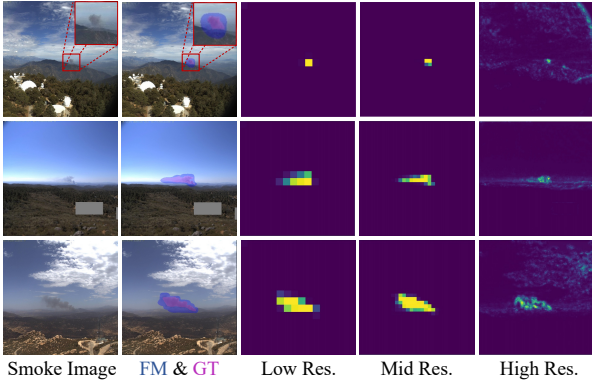


Figure 6. **Performances of Focus Module.** The Focus Map (FM & GT, The blue region represents the Focus Map, while the red denotes the ground truth.) can recognize small smoke and cover smoke of different scales. Low-resolution feature can help to cover the smoke body, while high-resolution feature provide detailed information about smoke edge.

be generated to fully cover the smoke area (GT) and suppress background interference.

Effect of Separation Module. Method (d) in Table 4 demonstrates the role of the Separation module. This method of separating the *smoke foreground* from a smoke-free background results in a notable increase in precision, particularly in the segmentation of small smoke particles, where precision improved by 7.87% compared to the baseline and by 8.30% compared to the focus module only. The

foreground feature in Fig. 7 demonstrates that the extracted smoke foreground feature closely resembles the shape of the smoke itself, particularly the fine edges of the smoke. To further explore the role of the foreground features, we conduct a experiment that only the foreground features are used for prediction in the decoder head. As shown in Table 5, the "Foreground only" method even outperforms the Segformer [26] which using the full original features on F_β metric. This demonstrates the immense potential of the foreground feature in our FoSp.

Effect of Domain Fusion Module. Method (e) in Table 4 has demonstrated the effectiveness of Domain Fusion. After incorporating the Focus module, the model is inclined towards improving recall, while adding the Separation module tends to improve precision. Furthermore, after including the domain fusion module, a better balance between these two metrics is achieved, resulting in the best performance on F_β metric. Compared to the baseline, the model shows a significant improvement of 4.09% (F_β) on the entire test set, and an even more pronounced improvement of 7.71% on the test set of small smoke particles.

4.5. Further Analysis

Feature-level Separation and Image-level Separation. Fig. 8 has shown the performance of the image-level separation. Although image-level separation methods can split the foreground of smoke more precisely, it is computation-

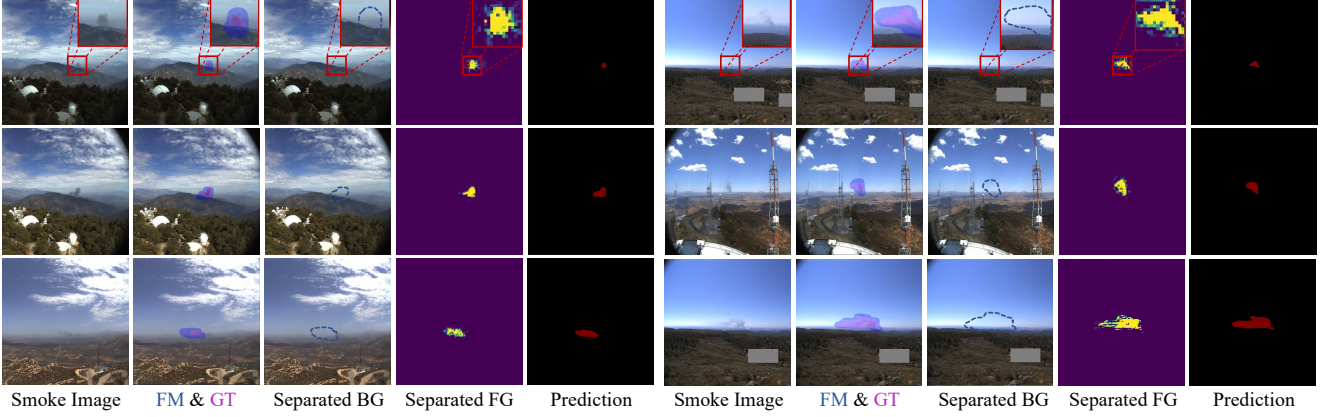


Figure 7. **Performances of Separation Module.** We have visualized the Focus Map and ground truth (FM & GT, The blue region represents the Focus Map, while the red denotes the ground truth.), the separated background image (Separated BG), the separated foreground features (Separated FG), and the prediction of FoSp. The separated background image is presented to demonstrate the effectiveness of separation which does not be used in training or testing. It can be observed that our Separation module can obtain finer foreground for both small and transparent smoke.

Method	$F_\beta \uparrow$	$mIoU \uparrow$	$\mathcal{M} \downarrow$
Segformer	67.99	54.98	0.0088
Foreground only	68.22	54.94	0.0087
FoSp (image-level)	71.04	57.81	0.0082
FoSp (feature-level)	72.05	59.03	0.0079

Table 5. Experiments on different separation level.

	FM Threshold	FM Recall	$F_\beta \uparrow$	$mIoU \uparrow$
Segformer	-	-	67.99	54.98
FoSp	0.9	42.53	69.79	55.58
FoSp	0.8	53.65	71.75	58.30
FoSp	0.7	62.40	71.52	58.40
FoSp	0.6	69.40	70.30	57.29
FoSp (ours)	0.15	88.74	72.05	59.03

Table 6. Experiments on different Focus Map thresholds.

ally expensive to restore the complete image, and down-sampling is required to match the feature dimension of the original image. We have conducted experiments on both feature-level and image-level separation methods, as shown in Table 5. It can be observed that the FoSp using image-level separation outperformed Segformer by 2.06% on F_β and 1.52% on $mIoU$, which first proves the effectiveness of the FoSp concept. However, compared to the feature-level separation FoSp, the image-level FoSp results in a lower F_β and $mIoU$. Therefore, we think feature-level separation is the optimal choice for our FoSp.

Situation When the Focus Map (FM) Can Not Cover Smoke. To measure the degree of FM’s coverage of smoke, we directly regard FM as the prediction and calculate its recall. In order to explore the situations where FM cannot cover the smoke, we increase the FM threshold. As presented in Table 6, we observe that the recall of FM decreases as the threshold value increases. However, even at a high threshold of 0.9, our FoSp can still reach 69.79% on F_β ,

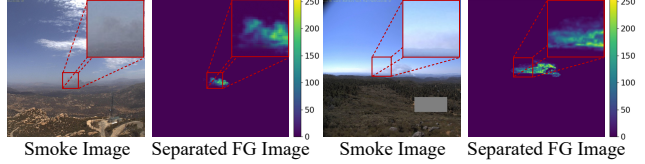


Figure 8. **Performances of image-level separation.** Image-level separation (Separated FG Image) can provide clearer transparency information on smoke edge compared to the original image. The lower the value, the higher the transparency.

higher than SegFormer [26]. Therefore, it demonstrates that even when FM can not cover the smoke completely, FoSp still performs well. Meanwhile, we select an FM threshold of 0.15 in our experiments and directly use FM as the prediction for testing. The recall reaches 88.74%, indicating that in most cases, our FM can cover the smoke.

5. Conclusions

In this paper, we propose a FoSp for early smoke segmentation (ESS). Concentrating on the formulation of smoke, we first determine the scope of the smoke, and then separate the pure smoke foreground from the smoke-free background, increasing the contrast between the background and foreground to obtain the complete and refined segmentation map. Furthermore, we provide a SmokeSeg dataset for ESS to promote the development of this field. Surprisingly, we find that sometimes using image-level separation can provide a certain degree of transparency information at the edges of smoke, as shown in Fig. 8. This has surpassed the scope of binary segmentation and we believe that this method can be applied to more sophisticated segmentation tasks such as image matting.

References

- [1] Liang-Chieh Chen, Yukun Zhu, George Papandreou, Florian Schroff, and Hartwig Adam. Encoder-decoder with atrous separable convolution for semantic image segmentation. In *Proceedings of the European conference on computer vision (ECCV)*, pages 801–818, 2018.
- [2] Anshuman Dewangan, Yash Pande, Hans-Werner Braun, Frank Vernon, Ismael Perez, Ilkay Altintas, Garrison W Cottrell, and Mai H Nguyen. Figlib & smokeynet: Dataset and deep learning model for real-time wildland fire smoke detection. *Remote Sensing*, 14(4):1007, 2022.
- [3] Henghui Ding, Xudong Jiang, Bing Shuai, Ai Qun Liu, and Gang Wang. Context contrasted feature and gated multi-scale aggregation for scene segmentation. In *Proceedings of the IEEE conference on computer vision and pattern recognition*, pages 2393–2402, 2018.
- [4] Yen-Chia Hsu, Ting-Hao Kenneth Huang, Ting-Yao Hu, Paul Dille, Sean Prendi, Ryan Hoffman, Anastasia Tsuhlares, Jessica Pachuta, Randy Sargent, and Illah Nourbakhsh. Project rise: recognizing industrial smoke emissions. In *Proceedings of the AAAI Conference on Artificial Intelligence*, volume 35, pages 14813–14821, 2021.
- [5] Zilong Huang, Xinggang Wang, Lichao Huang, Chang Huang, Yunchao Wei, and Wenyu Liu. Ccnet: Criss-cross attention for semantic segmentation. In *Proceedings of the IEEE/CVF international conference on computer vision*, pages 603–612, 2019.
- [6] Md Amirul Islam, Shujon Naha, Mrigank Rochan, Neil Bruce, and Yang Wang. Label refinement network for coarse-to-fine semantic segmentation. *arXiv preprint arXiv:1703.00551*, 2017.
- [7] Yang Jia, Hanrong Du, Haijuan Wang, Runyang Yu, Lianghui Fan, Gao Xu, and Qixing Zhang. Automatic early smoke segmentation based on conditional generative adversarial networks. *Optik*, 193:162879, 2019.
- [8] Guosheng Lin, Anton Milan, Chunhua Shen, and Ian Reid. Refinenet: Multi-path refinement networks for high-resolution semantic segmentation. In *Proceedings of the IEEE conference on computer vision and pattern recognition*, pages 1925–1934, 2017.
- [9] Jonathan Long, Evan Shelhamer, and Trevor Darrell. Fully convolutional networks for semantic segmentation. In *Proceedings of the IEEE conference on computer vision and pattern recognition*, pages 3431–3440, 2015.
- [10] Ilya Loshchilov and Frank Hutter. Decoupled weight decay regularization. *arXiv preprint arXiv:1711.05101*, 2017.
- [11] Mubarak Adam Ishag Mahmoud and Hong Ren. Forest fire detection and identification using image processing and svm. *Journal of Information Processing Systems*, 15(1):159–168, 2019.
- [12] Sachin Mehta, Mohammad Rastegari, Anat Caspi, Linda Shapiro, and Hannaneh Hajishirzi. Espnet: Efficient spatial pyramid of dilated convolutions for semantic segmentation. In *Proceedings of the european conference on computer vision (ECCV)*, pages 552–568, 2018.
- [13] Khan Muhammad, Jamil Ahmad, and Sung Wook Baik. Early fire detection using convolutional neural networks during surveillance for effective disaster management. *Neurocomputing*, 288:30–42, 2018.
- [14] Mahyar Najibi, Bharat Singh, and Larry S Davis. Autofocus: Efficient multi-scale inference. In *Proceedings of the IEEE/CVF international conference on computer vision*, pages 9745–9755, 2019.
- [15] Alejandro Newell, Kaiyu Yang, and Jia Deng. Stacked hourglass networks for human pose estimation. In *Computer Vision–ECCV 2016: 14th European Conference, Amsterdam, The Netherlands, October 11–14, 2016, Proceedings, Part VIII 14*, pages 483–499. Springer, 2016.
- [16] Chao Peng, Xiangyu Zhang, Gang Yu, Guiming Luo, and Jian Sun. Large kernel matters—improve semantic segmentation by global convolutional network. In *Proceedings of the IEEE conference on computer vision and pattern recognition*, pages 4353–4361, 2017.
- [17] Xuebin Qin, Zichen Zhang, Chenyang Huang, Chao Gao, Masood Dehghan, and Martin Jagersand. Basnet: Boundary-aware salient object detection. In *Proceedings of the IEEE/CVF conference on computer vision and pattern recognition*, pages 7479–7489, 2019.
- [18] Donald A Robinson. Smoke detection: Critical element of a university residential fire safety program. *Journal of the American College Health Association*, 27(5):265–66, 1979.
- [19] Robin Strudel, Ricardo Garcia, Ivan Laptev, and Cordelia Schmid. Segmenter: Transformer for semantic segmentation. In *Proceedings of the IEEE/CVF International Conference on Computer Vision*, pages 7262–7272, 2021.
- [20] Burak Uzkent, Christopher Yeh, and Stefano Ermon. Efficient object detection in large images using deep reinforcement learning. In *Proceedings of the IEEE/CVF winter conference on applications of computer vision*, pages 1824–1833, 2020.
- [21] Shidong Wang, Yaping He, Ju Jia Zou, Dechuang Zhou, and Jian Wang. Early smoke detection in video using swaying and diffusion feature. *Journal of Intelligent & Fuzzy Systems*, 26(1):267–275, 2014.
- [22] Wenguan Wang, Jianbing Shen, and Ling Shao. Video salient object detection via fully convolutional networks. *IEEE Transactions on Image Processing*, 27(1):38–49, 2017.
- [23] Yulin Wang, Kangchen Lv, Rui Huang, Shiji Song, Le Yang, and Gao Huang. Glance and focus: a dynamic approach to reducing spatial redundancy in image classification. *Advances in Neural Information Processing Systems*, 33:2432–2444, 2020.
- [24] Jun Wei, Shuhui Wang, and Qingming Huang. F³net: fusion, feedback and focus for salient object detection. In *Proceedings of the AAAI conference on artificial intelligence*, volume 34, pages 12321–12328, 2020.
- [25] Zhe Wu, Li Su, and Qingming Huang. Stacked cross refinement network for edge-aware salient object detection. In *Proceedings of the IEEE/CVF international conference on computer vision*, pages 7264–7273, 2019.
- [26] Enze Xie, Wenhai Wang, Zhiding Yu, Anima Anandkumar, Jose M Alvarez, and Ping Luo. Segformer: Simple and efficient design for semantic segmentation with transformers. *Advances in Neural Information Processing Systems*, 34:12077–12090, 2021.

- [27] Zhenda Xie, Zheng Zhang, Xizhou Zhu, Gao Huang, and Stephen Lin. Spatially adaptive inference with stochastic feature sampling and interpolation. In *European conference on computer vision*, pages 531–548. Springer, 2020.
- [28] Deng Xing, Yu Zhongming, Wang Lin, and Li Jinlan. Smoke image segmentation based on color model. *Journal on Innovation and Sustainability RISUS*, 6(2):130–138, 2015.
- [29] Siyuan Yan, Jing Zhang, and Nick Barnes. Transmission-guided bayesian generative model for smoke segmentation. 2022.
- [30] Chenhongyi Yang, Zehao Huang, and Naiyan Wang. Query-det: Cascaded sparse query for accelerating high-resolution small object detection. In *Proceedings of the IEEE/CVF Conference on Computer Vision and Pattern Recognition*, pages 13668–13677, 2022.
- [31] Changqian Yu, Jingbo Wang, Chao Peng, Changxin Gao, Gang Yu, and Nong Sang. Learning a discriminative feature network for semantic segmentation. In *Proceedings of the IEEE conference on computer vision and pattern recognition*, pages 1857–1866, 2018.
- [32] Chi Yuan, Zhixiang Liu, and Youmin Zhang. Learning-based smoke detection for unmanned aerial vehicles applied to forest fire surveillance. *Journal of Intelligent & Robotic Systems*, 93(1):337–349, 2019.
- [33] Feiniu Yuan, Zeshu Dong, Lin Zhang, Xue Xia, and Jinting Shi. Cubic-cross convolutional attention and count prior embedding for smoke segmentation. *Pattern Recognition*, 131:108902, 2022.
- [34] Feiniu Yuan, Lin Zhang, Xue Xia, Qinghua Huang, and Xuelong Li. A wave-shaped deep neural network for smoke density estimation. *IEEE transactions on image processing*, 29:2301–2313, 2019.
- [35] Feiniu Yuan, Lin Zhang, Xue Xia, Boyang Wan, Qinghua Huang, and Xuelong Li. Deep smoke segmentation. *Neurocomputing*, 357:248–260, 2019.
- [36] Yuhui Yuan, Xilin Chen, and Jingdong Wang. Object-contextual representations for semantic segmentation. In *Computer Vision—ECCV 2020: 16th European Conference, Glasgow, UK, August 23–28, 2020, Proceedings, Part VI 16*, pages 173–190. Springer, 2020.
- [37] Hang Zhang, Kristin Dana, Jianping Shi, Zhongyue Zhang, Xiaogang Wang, Amrith Tyagi, and Amit Agrawal. Context encoding for semantic segmentation. In *Proceedings of the IEEE conference on Computer Vision and Pattern Recognition*, pages 7151–7160, 2018.
- [38] Jing Zhang, Deng-Ping Fan, Yuchao Dai, Saeed Anwar, Fatemeh Sadat Saleh, Tong Zhang, and Nick Barnes. Uc-net: Uncertainty inspired rgb-d saliency detection via conditional variational autoencoders. In *Proceedings of the IEEE/CVF conference on computer vision and pattern recognition*, pages 8582–8591, 2020.
- [39] Zheng Zhang, Chengquan Zhang, Wei Shen, Cong Yao, Wenyu Liu, and Xiang Bai. Multi-oriented text detection with fully convolutional networks. In *Proceedings of the IEEE conference on computer vision and pattern recognition*, pages 4159–4167, 2016.
- [40] Hengshuang Zhao, Jianping Shi, Xiaojuan Qi, Xiaogang Wang, and Jiaya Jia. Pyramid scene parsing network. In *Proceedings of the IEEE conference on computer vision and pattern recognition*, pages 2881–2890, 2017.
- [41] Huajun Zhou, Xiaohua Xie, Jian-Huang Lai, Zixuan Chen, and Lingxiao Yang. Interactive two-stream decoder for accurate and fast saliency detection. In *Proceedings of the IEEE/CVF conference on computer vision and pattern recognition*, pages 9141–9150, 2020.